JOURNAL OF MATERIALS SCIENCE 32 (1997) 3541–3548

Heterogeneity, nucleation, shrinkage and bloating in sol–gel glass ceramics (the case of lithium aluminosilicate compositions)

E. BRUNETON*,‡, J. BIGARRÉ*,‡, D. MICHEL*, PH. COLOMBAN‡,§,¶
*Centre d'Etudes de Chimie Métallurgique, CNRS, 15 rue Georges Urbain, 94400 Vitry, France
‡Materials Department, Office National d'Etudes et de Recherches Aérospatiales, BP 72, 92322 Châtillon, France

Sintering of sol–gel powders often leads to porous samples despite the high reactivity of such powders. The influence of heterogeneity coming firstly from the use of different reagents as gel formers (Si and Al alkoxides) or of a mixed nature (Si–Al ester) and secondly from the hydrolysis–polycondensation route (mixing in anhydrous condition or pre-hydrolysis of the reagents) was studied for a lithium aluminum silicate composition using differential thermal analysis, expansion-shrinkage measurements and X-ray diffraction. The effects of the synthesis conditions on the microstructures is discussed from optical microscopy, scanning electron microscopy and metallurgical observations.

1. Introduction

Chemical routes to ceramic powders, and the sol–gel route in particular, are well known to allow the preparation of more homogeneous materials than the usual ball-milling process. This advantage originates in the mixing in the liquid state which homogenizes the reagents at the molecular scale. The gelation step may preserve this homogeneity, as far as the gel former is concerned. The hydrolysis–polycondensation of many metal alkoxides $M–(OR)_n$ leads to gels [1]. Typically, the gel composition is $MO_{2-x}(OH)_{2x} \cdot nH_2O$ and the product is amorphous. The polymeric network consists of a metal–oxygen framework stabilized by surface hydroxyl groups, leading to a water-logged meso(micro)porous structure [2]. Ionic and molecular species which do not participate in the ionocovalent network remain in the water and/or are absorbed at the network surface [3]. Thus heterogeneity on the nanometric scale may result from the composition, the reagents used and the synthesis. Densification occurs by dehydroxylation–condensation of the gel former network but sintering and phase crystallization may also depend on the reaction between the polymeric network and species located in the liquid logged in the pore or adsorbed at the pore surface [4]. For instance, if lithium aluminosilicate (LAS) compositions are considered, Al and Si elements are gel formers [3] whereas Li^+ ions remain in the liquid, soaking the porosity. This favours the formation on heating of a lithium-rich liquid phase at the surface of the Si–O–Al polymeric network. It is also well established that the hydrolysis of metal alkoxides is highly dependent on the metal. For instance, the hydrolysis of Al alkoxide occurs more rapidly than that of silicon alkoxide. Thus, various degrees of heterogeneity are expected on the nanometric scale according to the used reagents and their hydrolysis process. Various phases may nucleate from the intermediate amorphous mesoporous state originating from the thermal treatment of the gels and a polyphasic ceramic can be obtained instead of the expected single-phase material. Furthermore, irrespective of the attempts of glass makers to reach the highest homogeneity, the target of ceramists is more complex, owing to the polyphasic nature of glass–ceramics and most ceramics. Second phases may play an important (negative or positive) role on the physical and chemical properties of the ceramics and glass–ceramics and special microstructures may be required to obtain given properties.

In this paper, we report our investigation of LAS compositions. These materials with keatite (usually called β-spodumene) or high quartz (called δ-spodumene or β-eucryptite) structures form extensive solid solutions in the $Li_2O–Al_2O_3–SiO_2$ system [5, 6]. Because of their low densities, low thermal expansions and medium melting temperatures, these compounds are mainly used in the form of more or less recrystallized glass–ceramics as well as cooking table wares, heat exchangers and telescope mirrors in the form of monolithic pieces [6] as in gas turbines or jet engines in the form of composite matrices [7, 8]. In all cases, it is important to manufacture the material in the liquid phase, either from a liquid melt for the conventional fabrication route [9] or from a mixture

§Also at Laboratoire de Spectrochimie IR et Raman, CNRS, 2 rue Henri Dunant, 94320 Thiais, France.
¶Author to whom all correspondence should be addressed.

0022–2461

of alkoxide precursors for the sol–gel route [10]. We report here the influence of the molecular mixing (use of two different alkoxide precursors for Si and Al, and of a mixed Si–Al precursor) and the hydrolysis conditions (handling in a water-free atmosphere or not) on sintering. Emphasis will be given to understanding the bloating effects which are often observed as the main drawback of alkoxide sol–gel routes.

Upon heating, water and traces of remaining alcohol and unhydrolysed organic branches are lost and a glass-like material is obtained. As long as the protonic groups remain present, metal–hydroxyl bonds exist instead of metal–oxygen–metal bridges and a mesoporosity (or microporosity) appears [2]. Shrinkage results from the departure of protonic species which enhances a catastrophic densification of the polymeric network far before the softening of the material [11]. However, for glass-making compositions, bloating has been reported and related to the removal of gases through the viscous glass [12].

2. Experimental procedure

2.1. Sample preparation

The studied composition is $Li_2O–2Al_2O_3–4SiO_2$. Starting liquids used to prepare the gel are aluminium *sec*-butoxide (Al-*sec*-$(OBu)_3$) (from Alfa Ventron or Fluka) and tetraethylorthosilicate (TEOS) (from Alfa Ventron, Fluka or Hüls France, formerly Dynamit-Nobel) and *sec*-$(BuO)_2Al–O–Si(OEt)_3$ (SiAl diester) (from Hüls France, formerly Dynamit-Nobel). In this last compound, the Al–O–Si bond is soon present and this strongly decreases the hydrolysis rate [13]. This alkoxide can be handled in air which is not possible for the aluminium *sec*-butoxide owing to its very high hydrolysis rate. Consequently, the Al-*sec*-$(OBu)_3$ is first mixed with dry 2-propanol in a glove-box under argon where the water content is kept below 10 p.p.m. Rapid handling in air is then made possible, a plastic film being used to protect from the outside atmosphere.

The various routes used in this work are summarized in the flow charts shown in Fig. 1. In all cases, the alkoxide (or diester) to 2-propanol solvents molar ratio was 1 to 10 and the alkoxide(or diester)-to-water ratio corresponds to ten times the water volume required to obtain the stoichiometry hydrolysis. Previous studies have demonstrated that a large water excess is needed to obtain gel powder free of unhydrolysed branches and to avoid the crystallization of aluminium hydroxides [3, 14, 15].

2.1.1. Method a: two-gel-former water-free mixing route

Al-*sec*-$(OBu)_3$, $Si(OEt)_4$ and 2-propanol reagents were mixed in a glove-box. Stirring is maintained for 1 h at 75 °C before and after mixing in order to favour *trans*-esterification and hence to regulate the hydrolysis rate. The mixture is transferred out of the glove-box into a reactor vessel and an aqueous solution of lithium nitrate is added in order to obtain hydrolysis with the alkoxide-to-water volume ratio of 1 to 10 as indicated above. Vigorous mechanical stirring is maintained for 90 min in the glass reactor, which leads to the evaporation of most of the alcohols. The gel dispersion in water is then poured in a large plate and dried for 5–6 h under infrared bulbs. After that, a very fine white powder consisting of 0.1 μm aggregates is obtained.

2.1.2. Method b: two-gel-former atmosphere mixing route

The sample preparation is very similar except that the glove-box handling is used only for the Al-*sec*-$(OBu)_3$ and 2-propanol mixing. After that, the handling is carried out in air (i.e., with water traces). A plastic film

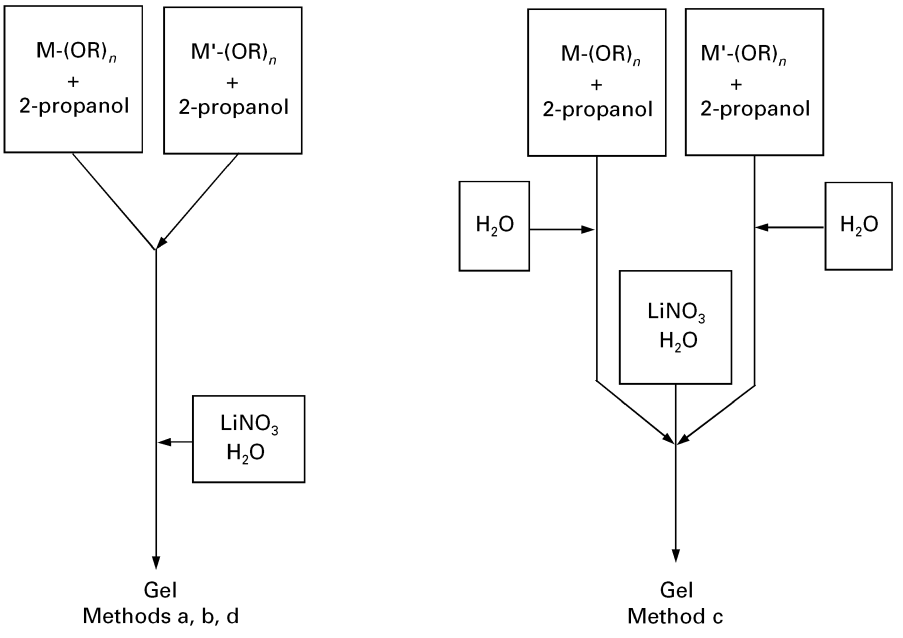

Figure 1 Flow charts for the preparation of LAS samples.

was used to cover the beaker. The alkoxide mixture became milky after agitation for $\frac{1}{2}$ h at 75 °C. After hydrolysis, a separation between the clear liquid and the gel particulates occurs in the plate before drying. Nevertheless, a white powder is finally obtained.

2.1.3. Method c: inhomogeneous route with two gel formers (diphasic method)

In this route, each alkoxide is mixed with 2-propanol for 1 h at 75 °C in a glove-box. Both mixtures are handled in air and hydrolysed separately in a large water excess, leading to two gel dispersions. These dispersions are then mixed together simultaneously with the lithium nitrate solution under vigorous stirring. After drying, a fine white powder is obtained.

2.1.4. Method d: homogeneous route with one gel former

This route is similar to route *a*, but the Al–Si diester is used. The Al–O–Si bonds present in this reagent improve chemical homogeneity.

2.2. Experimental techniques

Thermal expansion and shrinkage was studied up to 1200 °C using a DI 24 Adamel (Instrument SA, Longjumeau, France) apparatus designed for large variations in length. Gel pellets were pressed under a low stress (100 MPa) in order to highlight the sintering behaviour. Two heating rates were used. Differential thermal analysis (DTA) traces were recorded up to 1200 °C using a Dupont instrument. Absolute density and open porosity were determined by the Archimedes method. X-ray powder diffraction (XRD) diagrams were recorded with a Philips PW1710 automated diffractometer using a cobalt anticathode ($\lambda_{K\alpha} = 0.178\,89$ nm). Quantitative phase estimation was made by a comparison with reference aluminosilicate phases mixed in various proportions. The Li, Si and Al global chemical concentrations were checked by inductively coupled plasma analysis and gravimetry. The microstructure of the LAS glass–ceramics was observed on various scales with a Nikon optical microscope, a Zeiss DSM 950 scanning electron microscope and a 200 kV JEOL 200 FX transmission electron microscope. The relative local concentrations of silicon and aluminum was obtained from energy-dispersive X-ray analysis (EDX) by transmission electron microscopy (TEM) (Si:Li detector).

3. Results

3.1. Shrinkage behaviour

Shrinkage variations for samples prepared with the various methods are reported in Fig. 2. They have been recorded with two heating rates of 80 and 500 °C h^{-1}. The skeletal density, i.e., the density of the dense matter (including closed porosity) is given in Table I.

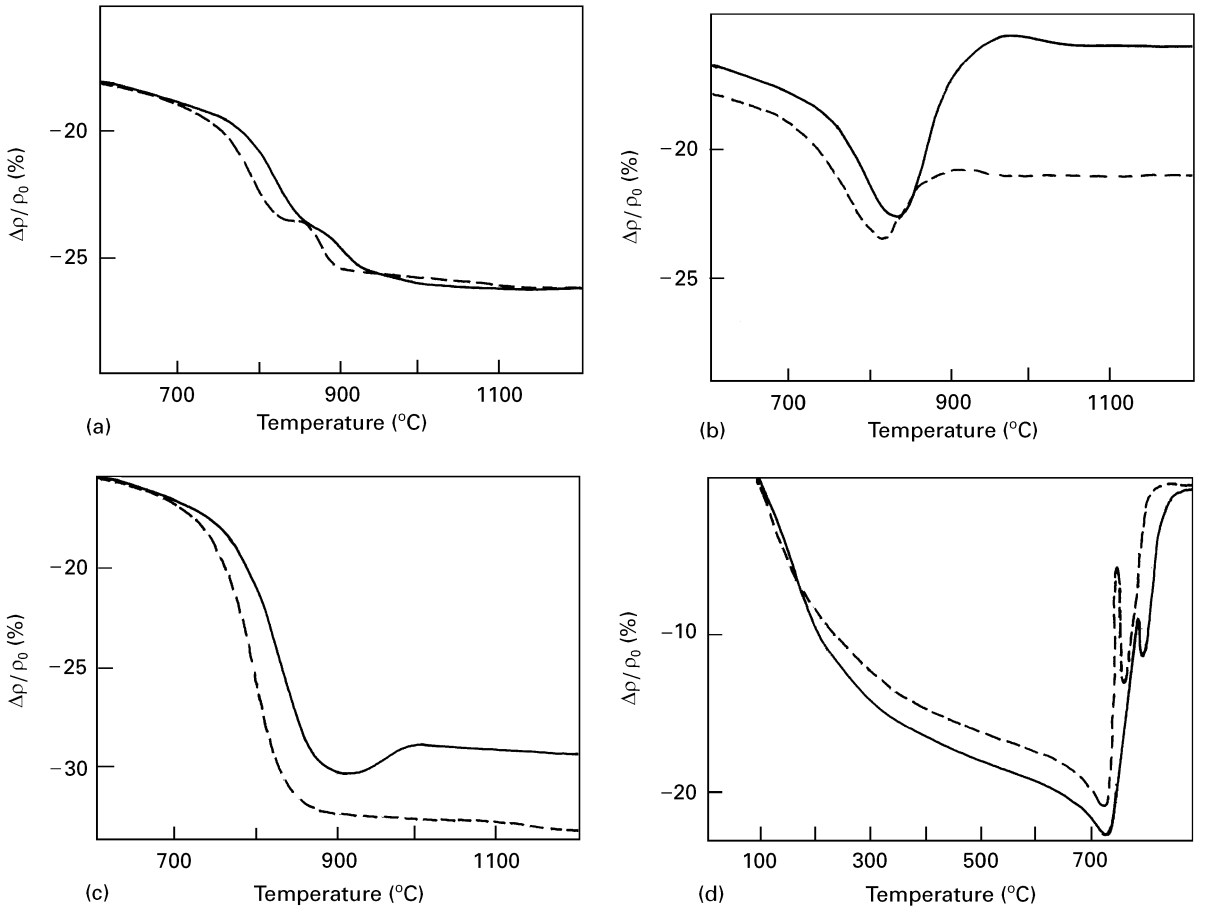

Figure 2 Dilatometric traces of LAS gels prepared by methods a, b, c and d recorded between room temperature and 1200 °C with two heating rates (——), 500 °C h^{-1}; (– – –), 80 °C h^{-1}.

TABLE I Skeletal density and open porosity of LAS sample prepared by different routes

Method	Sintering temperature[a] (°C)	Skeletal density[b] (g cm^{-3})	Open porosity (%)	Linear shrinkage[a] (%)	Main phases
a	800	2.2	8	22.5	Amorphous
	900	2.8	—	25.5	β-Eucryptite + mullite + amorphous
	1000	2.9	—	25.7	β-Eucryptite + mullite + amorphous
	1200	—	12	26.2	β-Spodumene + mullite
b	750	2.5	—	20.8	Amorphous
	800	2.6	12	24.2	Amorphous
	900	2.5	30	20.6	β-Eucryptite + amorphous
	1000	2.7	—	20.8	β-Eucryptite
	1200	—	14	20.8	β-Eucryptite + mullite
c	800	2.4	2	26	Amorphous
	1200	2.4	7	33	β-Eucryptite + mullite
d	700	2.3	17	19.8	Amorphous
	730	2.4	—	6	Amorphous + β-Eucryptite
	760	2.0	—	12	—
	800	2.3	—	1	β-Eucryptite + new phase
	1200	2.3	57	0	β-Eucryptite + mullite

—, not studied.
[a] 80 °C h^{-1} heating rate.
[b] Corresponds roughly to the absolute density.

Up to 600 °C, the relative shrinkages are very similar and reach about 20% from the initial state (see for instance Fig. 2d). Between 700 and 850–1000 °C, spectacular variations, still amplified when increasing the heating speed, are visible for the four samples. Then the stationary state is raised, giving the final densification. Before reaching this state, well-defined peaks are observed for the Al–Si route (Fig. 2d).

Bloating occurs for samples prepared with method b ("atmosphere mixing" route) and method d ("homogeneous" route). On the other hand, for samples prepared with method a ("water-free" route) and method c ("inhomogeneous" route), only a very low volume increase and some kinks appear during shrinkage (see Fig. 3 below). The main results can be summarized as follows.

3.1.1. "Water-free" method a

A final shrinkage of 26% is measured whatever the heating rate. A plateau between 830 and 850 °C with 80 °C h^{-1} heating rate and only a change in slope with 500 °C h^{-1} heating rate are first observed on the curves.

3.1.2. "Atmosphere mixing" method b

Shrinkage is only 21% (80 °C h^{-1}) or 16% (500 °C h^{-1}) above 1200 °C. Expansion effects of 1.5% between 830 and 900 °C (80 °C h^{-1}) and 7.5% between 830 and 960 °C (500 °C h^{-1}) are measured. The geometry remains then nearly constant except for a small densification in the 950–1000 °C range.

3.1.3. "Inhomogeneous" method c

This "diphasic" compound gives the highest densification: linear shrinkages of 29.5% and 33% with 80 °C h^{-1} and 500 °C h^{-1} heating rates respectively. At about 900 °C, the shrinkage is over even though a slight increase (approximately 0.5%) is observed up to 1200 °C with 80 °C h^{-1} heating rate.

3.1.4. "Homogeneous" method d

The contraction is 20% (80 °C h^{-1}) and 23% (500 °C h^{-1}) at 720 °C. Then, an expansion peak of 15% at about 740 °C followed by dilatation leads to a net shape sintering, i.e., 0% final shrinkage.

3.2. Sample densities

After thermal treatments (80 °C h^{-1} heating rate) at various temperatures in air, skeletal densities and open porosities are measured and samples are analysed by XRD. The skeletal densities displayed in Table I represent the average of several measurements. Dispersion is less than 10%.

Comparison of open porosity gives evidence of huge bloating occurring for samples prepared by methods b and d (open porosity, greater than 30%).

3.3. Crystallization and phase transformation

For all methods, crystallization does not start below 700 °C as usually observed in gels obtained by hydrolysis of these alkoxides. Then, the crystallized phases depend on the preparation as shown in Fig. 3.

3.3.1. Method a

The earliest crystallization stage takes place near 845 °C (Fig. 4a) as β-eucryptite starts to grow (Fig. 4a). This corresponds to a plateau on the shrinkage curve (Fig. 2a). The interplanar distance of the most intense XRD peak ($d_{010} = 0.351$ nm) is very close to that of the stoichoimetric Li_2O–Al_2O_3–$2SiO_2$

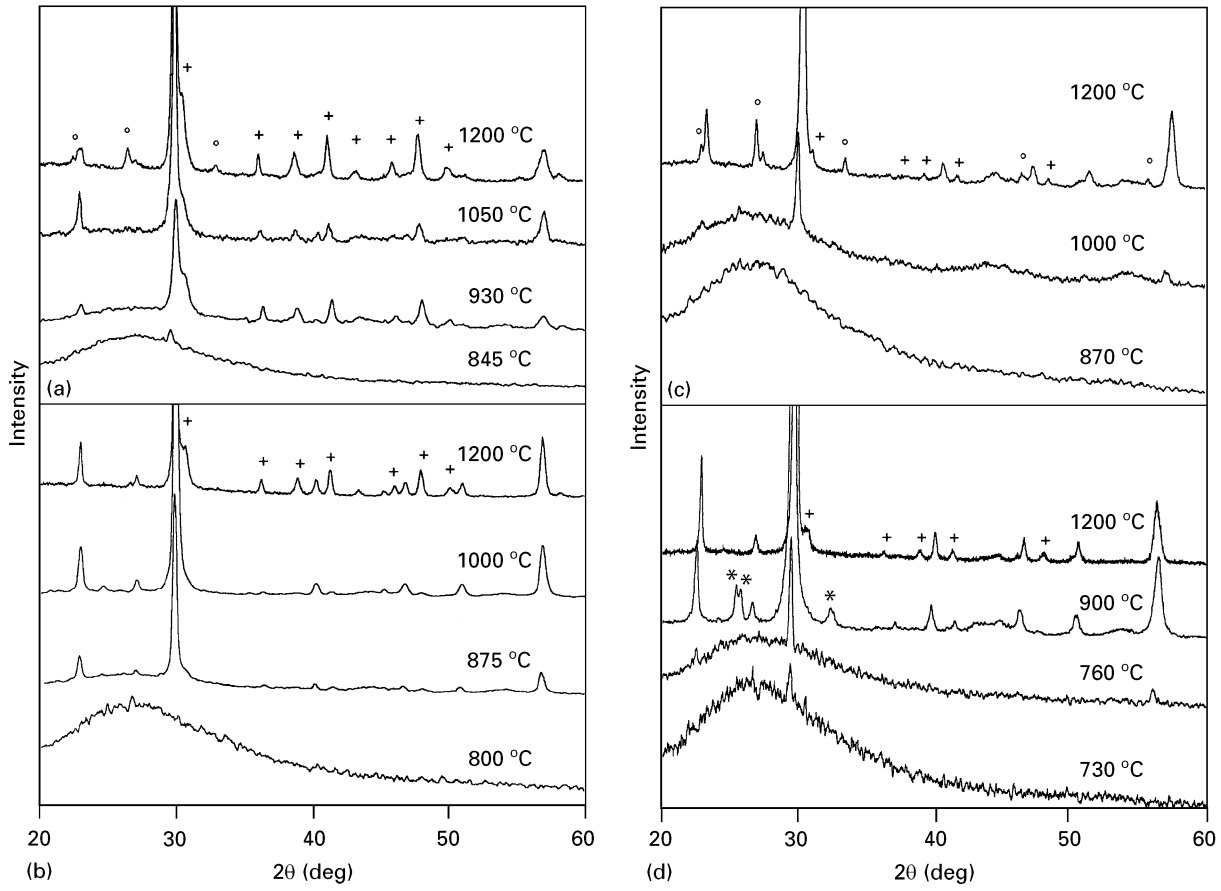

Figure 3 Variation in XRD patterns with annealing temperature for samples prepared by methods a, b, c and d. (○), β-spodumene; (+), mullite; (∗), metastable phase; other lines correspond to β-eucryptite.

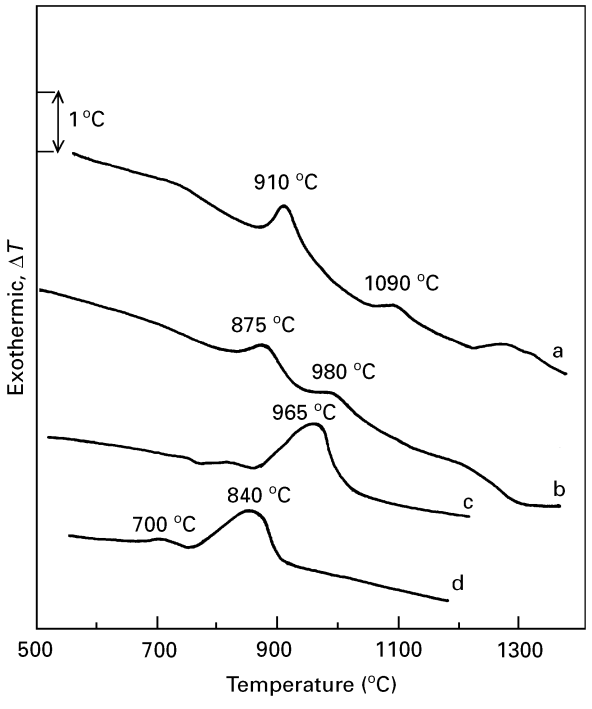

Figure 4 DTA curves of LAS gels prepared by methods a, b, c and d recorded between 600 and 1200 °C. The heating rate was 20 °C h^{-1} and the experiment was conducted in air.

composition ($d_{010} = 0.353$ nm) [16]. At the same temperature, or a few degrees Celsius higher, a mullite phase appears. Its composition is estimated to $3Al_2O_3$–$2SiO_2$ from the values of the lattice constant compared with literature data [17–19]. The crystallization temperature of this aluminosilicate is generally about 1000 °C when prepared by hydrolysis–polycondensation of alkoxides [2, 15, 17, 18]. Lower nucleation temperatures have been sometimes observed [17–22] within the range of formation of disordered mullite which extends from about $2Al_2O_3$–$3SiO_2$ to $9Al_2O_3$–SiO_2 with these synthesis routes. The exothermic peak at 910 °C in DTA (Fig. 4) should probably be assigned to the crystallization of these two phases which are the only crystallized products observed up to 1000 °C. However, these crystals are embedded in the untransformed glassy matrix as shown in Fig. 5a. At higher temperatures a large amount of mullite remains present and the keatite β-spodumene is formed to the detriment of the high-quartz β-eucryptite which becomes unstable [23–26]. This phase transformation could be associated with the exothermic peak on the DTA curve near 1090 °C.

3.3.2. Method b

The sample remains completely amorphous at 800 °C, but EDX analysis reveals fluctuations in the Al-to-Si ratio in the amorphous sample. The first exothermic DTA peak appears at 875 °C (Fig. 4b). After a 30 min anneal at this temperature, XRD results show mullite traces and a β-eucryptite phase close to the stoichiometric composition. The expansion observed (Fig. 2b) can be related to the formation of β-eucryptite as in method a. However, the sample is not

completely crystallized at 875 °C as shown by a broad maximum in the background of the XRD spectrum. At 1000 °C, mullite is not detected any longer and well-defined β-eucryptite crystals are observed in addition to the glassy matrix (Fig. 5b).

Mullite traces appear at higher temperature after annealing with a β-eucryptite-to-mullite ratio of 85 to 15 at 1200 °C. The second exothermic DTA peak at about 1000 °C thus corresponds to the mullite formation. In this case, the crystallization temperatures of β-eucryptite and mullite fit well those usually found for these compounds [17, 18]. The β-eucryptite-to-β-spodumene transformation is not observed in this case. Finally, a noticeable glass amount is still observed by TEM at 1200 °C. Fig. 5b shows that the crystallization process is also not achieved for the corresponding sample obtained by route a.

3.3.3. Method c

The amorphous phase remains amorphous up to the exothermic DTA peak at 965 °C (Fig. 4c) which corresponds to the crystallization of β-eucryptite (Fig. 3c). At 1000 °C, the specimen is still poorly crystallized. This delayed crystallization can be correlated to the use of a diphasic gel. At 1100 °C, a low amount of mullite (less than 5 mol%) is formed and β-eucryptite has been mostly transformed into β-spodumene. A small exothermic peak occurs at this temperature.

3.3.4. Method d

The crystallization temperature of β-eucryptite which is especially low in this case is associated with a weak DTA peak at 700 °C (Fig. 4d). The second exothermic peak at 840 °C is rather intense and does not correspond to mullite formation nor to the eucryptite-to-spodumene transformation, but to an unidentified other phase appearing in XRD patterns. This effect is probably responsible for the second expansion occuring between 750 and 800 °C. This phase has completely disappeared at 1200 °C and only β-eucryptite and mullite traces (more than 1 mol%) are detected. Except for the formation of the metastable compound,

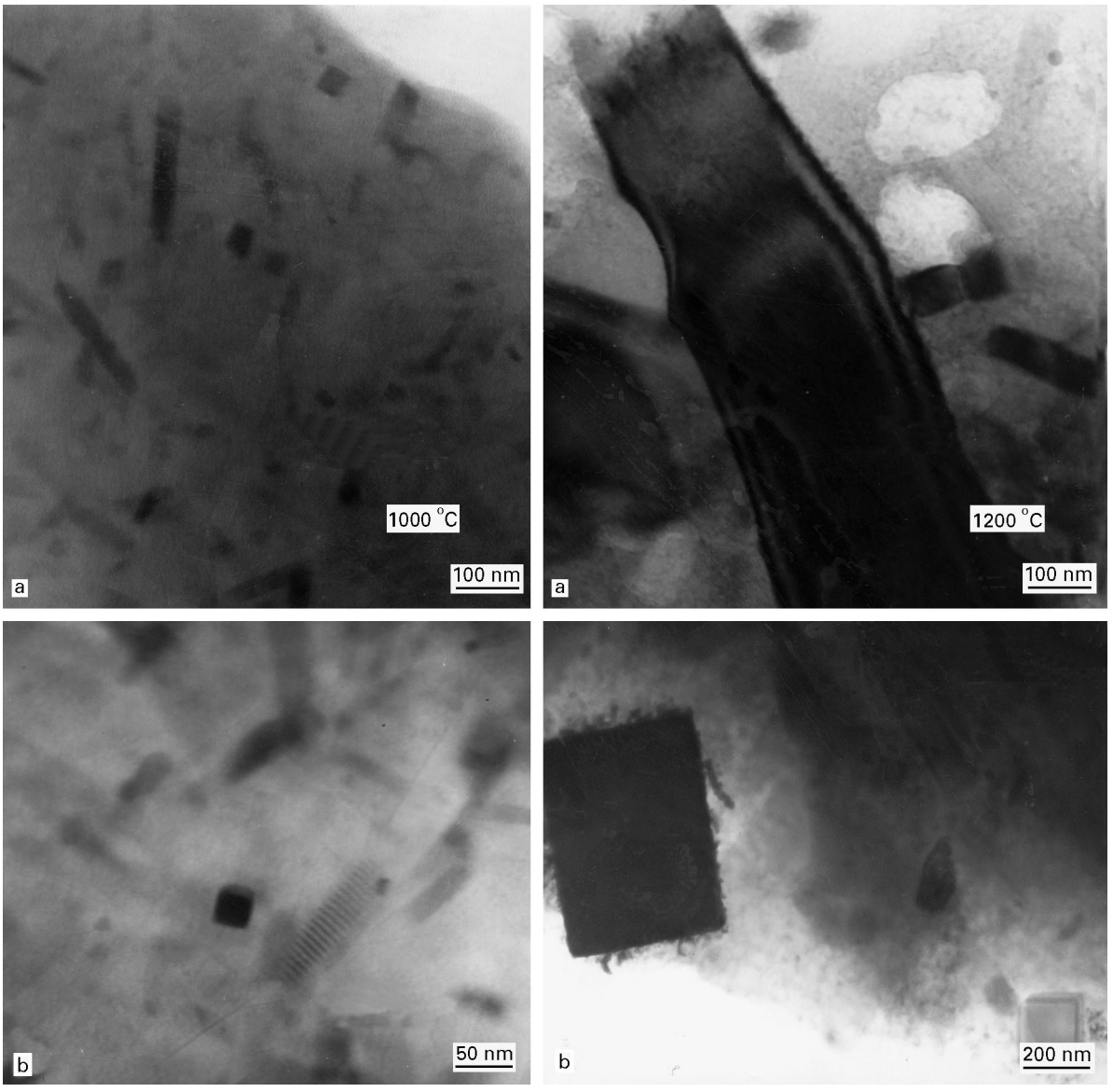

Figure 5 Transmission electron micrographs of a LAS sample prepared by methods a and b, after annealing at 1000 °C (left) and 1200 °C (right). Small acicular crystals are mullite and β-eucryptite and the well-contrasted crystal (top right) is a mullite needle.

an analogy can be made with the sample prepared by method b where the crystallization temperature of β-eucryptite is quite low and where no β-spodumene is observed.

4. Discussion

4.1. Microstructure

Microcracks and open porosity after annealing were studied by optical microscopy. The number and the shape of pores provides information about the shrinkage mechanism and microcracks can be often correlated to the presence of phases having different thermal expansion coefficients.

4.1.1. Method a

A low open porosity is displayed at 800 °C (Fig. 6a). Nevertheless, the glassy phase contains some microcracks. EDX as with a microprobe size about 100 nm show that the relative Al-to-Si ratio differs from one place to another. At 1200 °C, the number of microcraks increases as the same time as the (mullite + β-spodumene)-to-β-eucryptite ratio (Fig. 5b). The thermal expansion coefficient of β-eucryptite ($-9\times10^{-6}\,K^{-1}$) is negative and therefore much smaller than those of mullite ($4\times10^{-6}\,K^{-1}$) and β-spodumene ($1\text{–}2\times10^{-6}\,K^{-1}$) [8, 27].

4.1.2. Method b

At 800 °C, the open porosity is larger than in the previous case (Fig. 6b). The pores have generally a circular shape and are connected (Fig. 7). The bloating may result from the release of gases arising from the departure of hydroxyl (OH^-) groups which occurs up to 800–1000 °C in aluminosilicate xerogel [2]. It is likely that at this moment a viscous phase exists which explains the bloating and the spherical shape of the pores. The softening occurs at a relatively low temperature about (700–900 °C) and may be related to the formation of unstable and locally Li-rich phases.

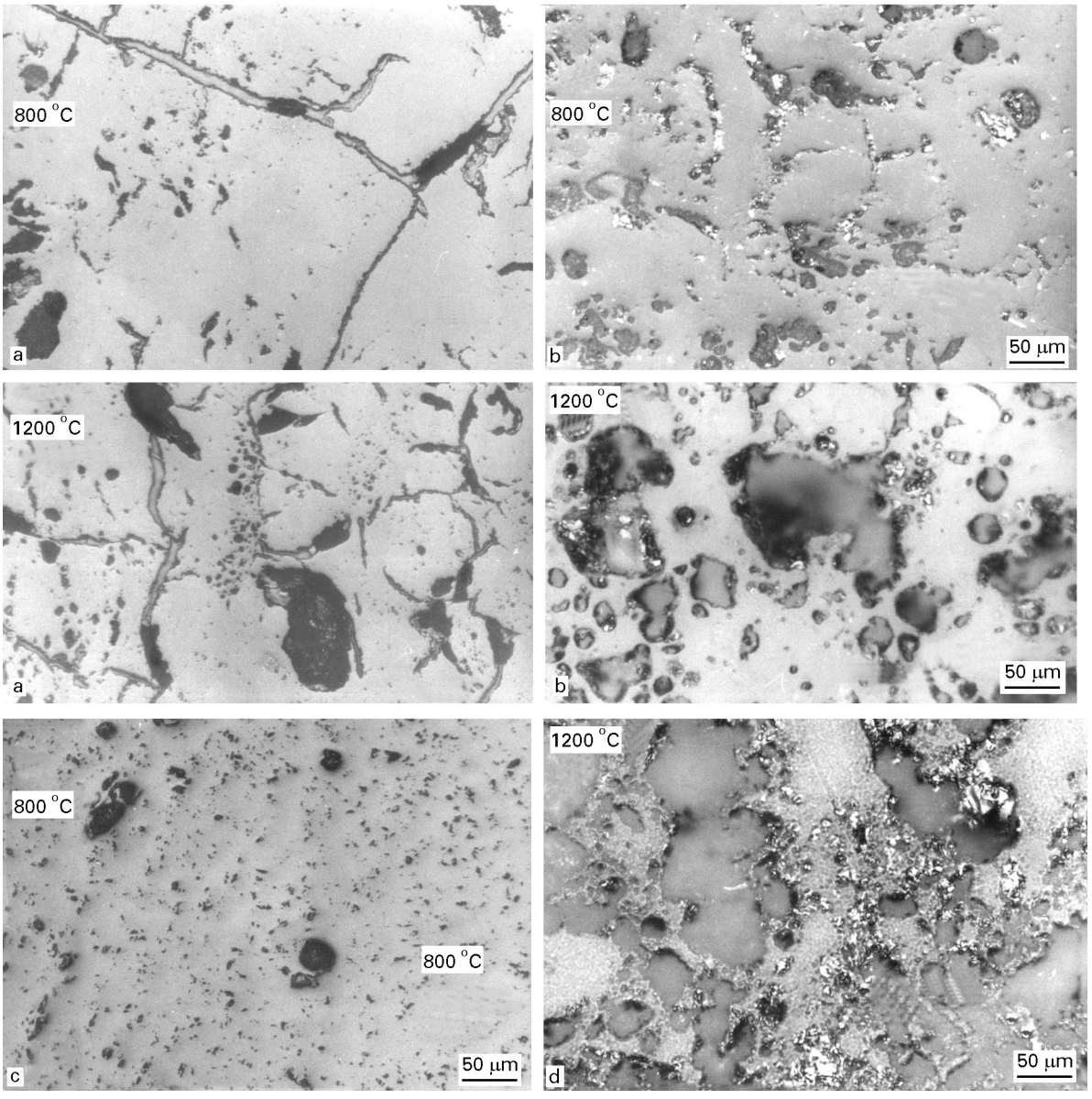

Figure 6 Optical micrographs of samples prepared by methods a, b and c after annealing at 800 °C and by methods a, b and d after annealing at 1200 °C.

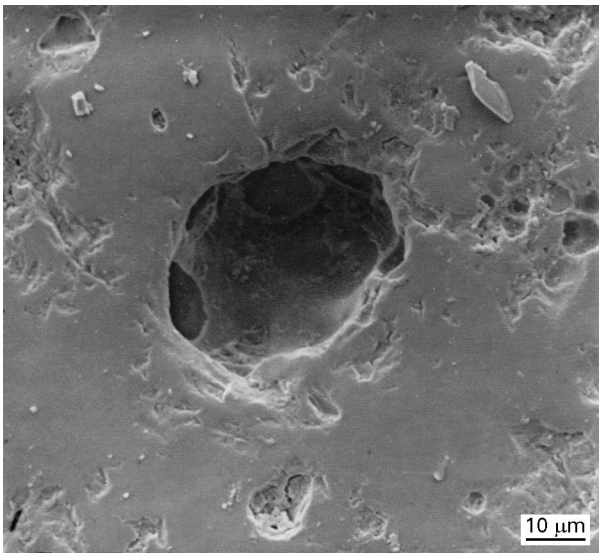

Figure 7 SEM image of connected pores in a LAS sample prepared by method b after annealing at 1200 °C.

Consequently, the amount of microcracks at 800 °C and even at 1200 °C is low (Fig. 6).

4.1.3. Method c

As mentioned in Section 3.1, porosity is very low after annealing at 800 °C. Therefore, only a few holes are observed in the optical image (Fig. 6c) and no cracks are visible.

4.1.4. Method d

Samples look like those synthesized by method b with interconnected pores.

5. Conclusions

Shrinkage of LAS-type compounds prepared by hydrolysis–polycondensation of alkoxide precursors leads to bloating effects during heating. This behaviour is attributed to the removal of water gaseous species in the presence of a transient Li-rich viscous phase. Crystallization of β-eucryptite (hexagonal high-quartz phase) which possesses a lower density [2, 4] than the generating glass [2, 27] is simultaneously observed.

With single-phase compositions, the densification of xerogels is usually associated with the nucleation of the crystalline phase when the departure of the hydroxyl groups reaches the metastability threshold. For all compositions studied in this paper, densification starts about 700 °C. Xerogels prepared using homogeneous routes (methods a and b) with two gel formers prepared in a more or less anhydrous atmosphere lead to materials with a large amount of amorphous phases. The presence of water traces probably favours first the hydrolysis of aluminium *sec*-butoxide and hence local heterogeneity which delays the crystallization of β-eucryptite. This effect is larger for the diphasic preparation (method c) for which β-eucryptite is found above 900 °C only. This shift in crystallization temperature out of the densification step gives better sinterability. The use of two precursors for Al and Si elements also gives a rather good sinterability if the mixing process is made in a water-free atmosphere. Crystallization occurs simultaneously with densification but a large amount of mullite is formed in this case. On the other hand, highly homogeneous mixing of Al and Si elements promotes the formation of β-eucryptite at very low temperatures (about 700 °C) at the beginning of the skeleton densification. This stops densification and the presence of a liquid phase containing Li ions which does not belong to the xerogel network leads to volume expansion and bubble formation.

References

1. L. C. KLEIN (ed.), "Sol–gel technology for thin films, fibers, preforms, electronics and specialty stages", (Noyes Publications, Parkridge, NJ, 1988).
2. PH. COLOMBAN and V. VENDANGE, *J. Non-Cryst. Solids* **146–147** (1992) 245.
3. PH. COLOMBAN, *Ceram. Int.* **15** (1989) 23.
4. *Idem.*, *Adv. Ceram.* **21** (1987) 139.
5. R. HATCH, *Amer. Mineral.* **28** (1993) 471.
6. H. SCHEIDLER and E. RODEK, *Ceram. Bull.* **68** (1989) 1926.
7. F. K. KO, *ibid.* **68** (1989) 401.
8. G. PARTRIDGE, *Angew. Chem. Int. Engng. Adv. Mater.* **328** (1989) 1746.
9. K. M. PREWO and J. J. BRENNAN, *J. Mater. Sci.* **17** (1982) 2371.
10. PH. COLOMBAN, M. MENET, E. MOUCHON, C. COURTEMANCHE and M. PARLIER, Fr. Patent 2672283, 4 February (1991); Eur. Patent 92400235.5; US Patent 07/830904.
11. V. VENDANGE and PH. COLOMBAN, *J. Sol–Gel Sci. Technol.* **2** (1994) 407.
12. M. PRASSAS and L. L. HENCH, in "Ultrastructure processing of ceramics and glasses", edited by L. L. Hench and D. R. Ulrich (Wiley, New York, 1984) pp. 100–25.
13. J. C. POUXVIEL and J. P. BOILOT, *J. Non-Cryst. Solids* **103** (1988) 331.
14. B. YOLDAS, *J. Mater. Sci.* **14** (1979) 1843.
15. PH. COLOMBAN, *ibid.* **24** (1989) 3011.
16. C. T. LI, *Z. Kristallogr.* **127** (1968) 327.
17. PH. COLOMBAN and L. MAZEROLLES, *J. Mater. Sci. Lett.* **2** (1990) 1077.
18. *Idem.*, *J. Mater. Sci.* **26** (1991) 3503.
19. W. E. CAMERON, *Amer. Ceram. Sci. Bull.* **56** (1977) 1003.
20. T. BAN, S. HAYASHI, A. YASUMORI and K. OKADA, *J. Eur. Ceram. Soc.* **16** (1996) 127.
21. J. C. HULING and G. L. MESSING, *J. Non-Cryst. Solids* **147–148** (1992) 213.
22. R. X. FISCHER, H. SCHNEIDER and D. VOLL, *J. Eur. Ceram. Soc.* **16** (1996) 109.
23. C. T. LI and D. R. PREACOR, *Z. Kristallogr.* **126** (1968) 46.
24. P. T. CLARK and J. M. SPINK, *ibid.* **130** (1969) 420.
25. A. ZIADI, J. P. MERCURIO and B. FRIT, *Mater. Res. Bull.* **19** (1984) 1015.
26. J. Y. HSO and R. F. SPEYER, *J. Amer. Ceram. Soc.* **72** (1989) 2334.
27. S. KNICHERBOCHER, M. R. TUZZOLO and S. LAWHOME, *J. Amer. Ceram. Soc.* **72** (1989) 1873–79.

Received 10 October 1995
and accepted 20 January 1997